



Nanosized amorphous (Co, Fe) oxide particles decorated PANI–CNT: facile synthesis, characterization, magnetic, electromagnetic properties and their application

Farhood Heydari¹ · Seyyed Salman Seyyed Afghahi² · Mehrdad Manteghian³ · Mohammad Javad Taghizadeh⁴

Received: 24 March 2017 / Accepted: 15 November 2017 / Published online: 22 November 2017
© The Author(s) 2017. This article is an open access publication

Abstract

In this research (PANI/CNT) core/shell nanocomposite were synthesized via in situ chemical oxidative seeding polymerization, the results of SEM indicated the structure of synthesized nanocomposite. TEM, FTIR, UV–Vis, XRD analyses of samples showed that this nanocomposite is decorated with (Fe, Co) oxide nanoparticles. The VSM test of as prepared and annealed nanocomposite exhibited the saturated magnetization of 1.1 and 3.86 emu/g, respectively; the coercivity values were also – 350 and – 110 Oe, respectively. The reflection loss characteristics of (Fe, Co) oxide–PANI–CNT core/shell nanocomposite were also investigated with a vector network analyzer, in the 8.2–12.4 GHz range (X band). The maximum absorption increases with enhancement of the dispersed nanoparticles percent in polyurethane matrix from 1 to 10%. The value of the maximum reflection loss in the absorption samples with 1 and 10% of nanoparticles is – 2.14 dB at 9.33 GHz and – 7.32 dB at 11.97 GHz, respectively.

Keywords Seeding polymerization · Co-precipitation · Magnetic properties · Microwave absorption

Introduction

The microwave absorbing materials have been greatly used in the masking technology of aircraft, television image interference of the tall buildings and microwave dark-room as well as electromagnetic interference (EMI) [1–4]. In the last four decades, conducting polymers (CPs) have gained a special status owing to wealth of applications [5–8]. Shielding and microwave absorption properties of these polymers can be explained in terms of electrical conductivity and presence of bound/localized charges (polarons/bipolarons) leading to strong polarization and relaxation effects [9, 10]. Among

conducting polymers, polyaniline (PANI) is a good nominated for the microwave absorber material due to its easier synthesis, lower cost and interesting characteristics such as thermal and chemical consistency, Low density, manageable conductance and high conductivity at microwave frequencies [11–13]. It has been reported that the microwave absorbing property of conductive polymer absorbent can be modified at presence of iron oxide magnetic nanoparticles (Fe₂O₃) [14]. In comparison with metal and ferrites powders; Carbon nanotube is an absorbent material with lower density and excellent absorbing properties [15, 16]. In this research PANI-modified CNTs have been synthesized with facile chemical method [17–20], (Fe, Co) oxides were synthesized by reduction of Fe³⁺ and Co²⁺ ions on the surface of PANI branches at the presence of argon flow. Eventually, the magnetic and microwave absorbing properties of this nanocomposite were studied, which have not been reported in the previous publications.

✉ Farhood Heydari
farhod.heidari@modares.ac.ir

¹ Nanomaterials Group, Department of Materials Engineering, Tarbiat Modares University, Tehran, Iran

² Department of Engineering, Imam Hossein University, Tehran, Iran

³ Department of Chemical Engineering, Tarbiat Modares University, Tehran, Iran

⁴ Department of Chemistry, Imam Hossein University, Tehran, Iran



Experimental details

Materials

Aniline (Merck, Germany). Carbon nanotubes CNT, with length of 10–30 μm , external diameter 10–20 nm and surface area $> 200 \text{ m}^2 \text{ g}^{-1}$ were purchased from neutrino company. Hydrochloric acid (HCl, MP, Netherlands) and ammonium persulfate (APS, MP, Netherlands). $\text{FeCl}_3 \cdot 6\text{H}_2\text{O}$, $\text{Co}(\text{NO}_3)_2 \cdot 6\text{H}_2\text{O}$, NaBH_4 , NaOH and $(\text{CH}_2\text{OH})_2$ were purchased from MP Co. analytical grade of H_2SO_4 (MP, Netherlands), HNO_3 (MP, Netherlands), ethylene glycol (EG) and ethanol were purchased from pars chemistry.

Preparation

Preparation of CNT–PANI core shell

175 mL of mixed acid solution ($\text{HNO}_3/\text{H}_2\text{SO}_4$ 2:5 v/v) was prepared and 1 g CNT was dispersed in it; the mixed solution was ultrasonically agitated for 6 h at 90 °C. Subsequently the suspension was filtered and washed by deionized water until its pH value got close to 5. Then CNT powder was collected and dried in a vacuum at 80 °C. In the following, 1 g CNT was dispersed in 50 cc aqueous solution containing 3.77 cc HCl, the suspension agitation has been done by bath ultrasonic for 30 min and during this time 7.04 cc aniline was added dropwise to the suspension, after that the mixture was stirred continuously in ice bath (0–4 °C) and the polymerization was initiated by the dropwise addition of ammonium persulfate [0.06 g $(\text{NH}_4)_2 \text{S}_2\text{O}_8$ in 100 mL distilled water] and mixing was continued for 12 h. The reaction mixture was then filtered and washed repeatedly with distilled water and ethanol. The obtained wet CNT–polymer cake was dried at 60 °C for 2 h under dynamic vacuum condition.

Preparation of (Co, Fe) oxide nanoparticles decorated PANI–CNT

For a typical reaction, 30 mg PANI–CNT, 110 mg $\text{FeCl}_3 \cdot 6\text{H}_2\text{O}$ and 110 mg $\text{Co}(\text{NO}_3)_2 \cdot 6\text{H}_2\text{O}$ were charged into 50 mL EG, suspension agitating was done by bath ultrasonic for 30 min. 162 mg sodium hydroxide and 780 mg sodium borohydride were solved in 10 mL EG and this solution was then slowly added to the salt solution drop wise under argon flow in 30 min, the reaction was performed at 80 °C for 2 h under stirring. The prepared precipitate was then centrifuged at 2000 rpm to separate it from the top liquid, then the nanoparticles were washed with ethanol. Finally, the nanocomposite dried at 60 °C for 2 h under dynamic vacuum. Slightly

of the dried sample was then annealed at 600 °C for 1 h under argon blow to get the desired crystalline nanoparticles.

Characterization

The infrared spectra of powdered samples were taken at resolution of 4.0 cm^{-1} in $400\text{--}4000 \text{ cm}^{-1}$ range, using NICOLET 5700 FTIR spectrophotometer. UV–Vis absorbance spectra were recorded on a PerkinElmer UV spectrophotometer. Morphologies were observed using SEM (Leo 440, UK) and TEM (JEM-2100 Jeol, Japan). Powder X-ray diffraction (XRD) patterns of the samples were collected on an X-ray diffractometer (D8 ADVANCE, Bruker, Ltd., Germany) using $\text{Cu } \alpha$ radiation. The measurements were made at 40 kV, 40 mA, and intervals of $0.02^\circ \text{ s}^{-1}$ with a time step of 0.5 s over the range of $10^\circ < 2\theta < 80^\circ$. Magnetic hysteresis loops were recorded at room temperature using of a vibrating sample magnetometry (VSM; LAKESHORE VSM 7404, Lake Shore Cryotronics, Inc., USA) with a maximum magnetic field of 8.5 kOe. The EMI shielding measurements were taken on pressed rectangular pellets (2 mm thick) placed inside the sample holder. The holder matches the internal dimensions of Ku band (12.4–18 GHz) waveguide placed between the two ports of Vector Network Analyzer (VNA E8263B Agilent Technologies).

Results and discussion

Microstructural characterization

FTIR spectra analysis

Figure 1a shows the FTIR spectra of (Fe, Co) oxide–PANI–CNT nanocomposite. Characteristic bands at 1111 and 1617 cm^{-1} correspond to the stretching modes of vibration for the C–C and C=C bonds, respectively, which can be attributed to CNT or PANI structure. Characteristic bands at 1453 cm^{-1} correspond to the C=C stretch in the quinoid and benzenoid structure of PANI. Also the bands at 1276 cm^{-1} are assigned to the C–N stretching mode of benzenoid units. According to the results, the existence of PANI in the form of emeraldine salt is confirmed [21]. Bands at 1390 and 3427 cm^{-1} are related to the carboxylic acid groups created on the surface of CNT, and the band at 1010 cm^{-1} is assigned to O–H deformation vibrations [22]. The 1276 cm^{-1} bands are assigned to the asymmetric C–N stretching modes of polaron structure of PANI [23]. peaks observed in positions 440 and 594 cm^{-1} are attributed to the vibration of iron and cobalt ions, These peaks have slight difference with the values reported in previous research [24].

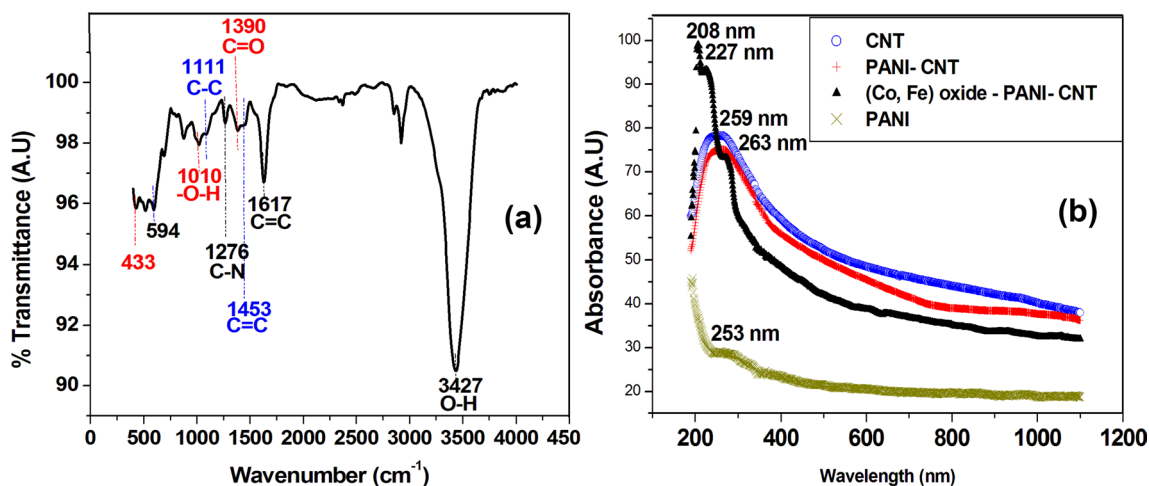


Fig. 1 FTIR spectra of (Fe, Co) oxide–PANI–CNT nanocomposite (a) and UV–Vis spectra of CNT, PANI, PANI–CNT and (Fe, Co) oxide–PANI–CNT nano composite (b)

UV–visible spectra analysis

The UV–Vis spectra of the CNT, PANI, PANI–CNT and (Fe, Co) oxide–PANI–CNT nanocomposites are shown in Fig. 1b. The peaks at 259 and 253 nm are related to CNT and PANI, respectively. The PANI–CNT composite demonstrated a peak at 263 nm and it was shifted by 4 and 10 nm compared to CNT and PANI spectra, respectively; which can be due to the interplay interfacial between PANI and CNT and approves the incorporation of functionalized CNTs in PANI chain. This furthermore shows that the interplay among the CNT and PANI layer makes electron delocalization between the nanocomposite easier and leads to increase of polymer electrical conductivity [25]. The UV–Vis spectroscopy results of Fe, Co and O doped PANI–CNT showed peaks in 208 and 227 nm, indicating augmentation of light absorption in the UV range and increase of bandgap energy of PANI–CNT by incorporation of transition metals (Fe, Co) and O under UV light irradiation.

Morphological and quantitative details

Figure 2a shows the SEM images of PANI–CNT nanocomposites; as it can be seen, The PANI–CNT nanocomposites have uniform morphology. SEM images obviously show that the PANI–CNT nanocomposites have coaxially tube shaped structures with a coating on the surface of tube perimeter. From the TEM images (Fig. 2c, d) it could be seen that on the surface of PANI–CNT; (Fe, Co) oxide nanoparticles were aggregated together to form large clusters. Plotted in Fig. 2e is the size distribution of particles on the surface of PANI–CNT nanocomposites. A really narrow size distribution of the magnetic nanoparticles is found, with sizes mostly falling between 7.0 and 9.0 nm. Utilizing of

PANI-*g*-MWNTs as the supporting materials causes uniform distribution of (Fe, Co) oxide nanoparticles on the outer surface of PANI-*g*-MWNTs with rather uniform particle sizes and prevention of magnetic nano particle agglomeration just as shown in Fig. 2b, d, the surface of PANI branches have favorite sites for nucleation and growing of (Fe, Co) oxide and render nanoparticles with bead-like morphology (Scheme 1).

XRD analysis

According to Fig. 3, only one peak is observed in pre annealing sample at position of $2\theta = 26.10^\circ$ which is related to the (002) reflection of CNTs in (Ni, Co) oxide–PANI–CNT hybrids [26], it is due to the amorphous magnetic nanoparticles. It is observed from diffraction pattern of annealed samples that the characteristic peaks at $2\theta = 18.23^\circ$ (440), 30.28° (511), 43.24° (400), 53.74° (311) and 62.89° (111) are matching the PDF2 00-001-1121 well and can be assigned to the CoFe_2O_4 NPs characteristic peaks. These patterns reveal good crystallinity and rather broad peaks due to smaller particle size. The crystallite size of the prepared nanocomposite was calculated using Scherer's formula:

$$d = \frac{k\lambda}{\beta \cos \theta}, \quad (1)$$

where d is crystallite size, β is the full width at half maximum of the most intense peak and K is an instrumental constant. The average crystallite sizes of CoFe_2O_4 is 9.35 nm. Hence, by considering the XRD plot and previous tests it can be resulted that the final materials are nanocomposite based on (Fe, Co) oxide (amorphous)–PANI–CNT and CoFe_2O_4 (crystalline)–CNT before and after annealing, respectively.



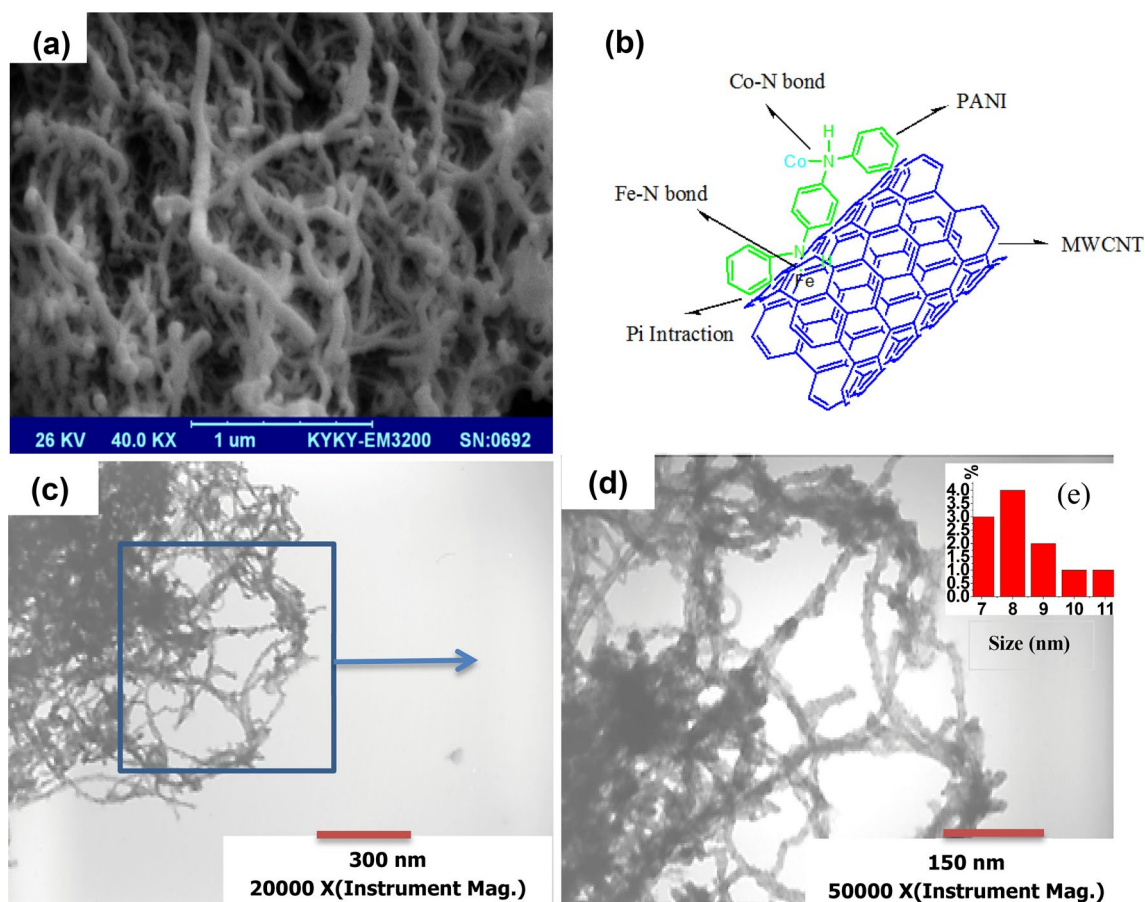
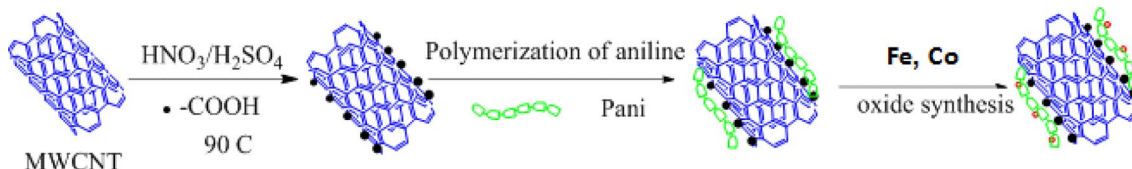


Fig. 2 SEM image of PANI–CNT core–shell nanostructure (a), schematic of the nanocomposite formation (b), TEM images of (Fe, Co) oxide–PANI–CNT structure (c, d), size distribution histogram of nanoparticles coated on the surface of PANI–CNT (e)



Scheme 1 Mechanism of the composite formation

Magnetic and electromagnetic analyses

VSM analyses

As it can be seen in Fig. 3a, Table 1, annealing led to increase of the magnetization intensity; and the sample exhibited ferromagnetic behaviors with soft magnetic feature and smaller H_c in comparison with amorphous (Fe, Co) oxide; its cause can be attributed to interactions between particles (Fig. 4b), in the sample annealed, particle density has been increased with atomic diffusion and thus the magnetic interactions between particles are increased. Cobalt

and iron are strong magnet therefore the field of A at C now aids the applied field, and C would reverse its magnetization at a lower applied field than if A were absent; the coercivity would therefore be lowered [27].

Furthermore, by annealing the saturation magnetization increased from 1.1 to 3.86 emu/g; in fact exchange interaction in ferromagnetic compounds is positive and spins are orientated in the parallel direction to each other. But when particle size is reduced; a remarkable percent of the atoms and spins are located on the surface of nanoparticles [28], neighborhood number of atoms on the surface is lower than the atoms inside nanoparticles and so magnetic

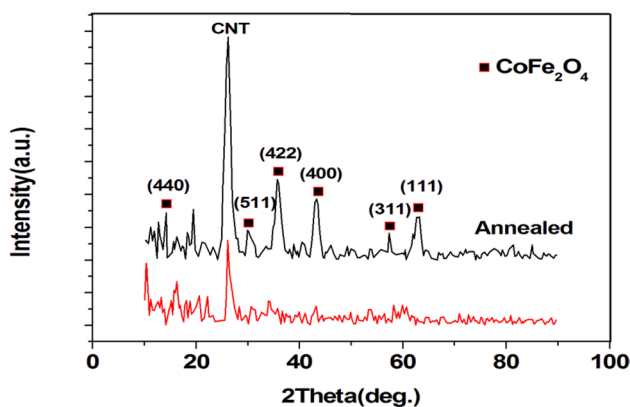


Fig. 3 XRD patterns of synthesized nanocomposite before and after annealing

Table 1 VSM analysis of synthesized nanocomposite

Sample	M_s (emu/g)	M_r (emu/g)	H_c (Oe)
Before annealing	1.1	0.24	– 350
After annealing	3.86	0.6	– 110

moments have a tendency to vibrate so as to cause lack of interaction coupling between of the magnetic dipole of atoms on the surface. So, spins irregularity produced a dead layer on the surface of nanoparticles [29]; with annealing and increased nanoparticles size, area of the dead layer decreased and as a result, with increase the total of the magnetic dipole moment, the saturation magnetization enlarges.

Analysis of the electromagnetic characteristics

Figure 5a–d depicts the variation of the electromagnetic characteristics: the complex permittivity ($\epsilon_r = \epsilon'_r + i\epsilon''_r$) and permeability $\mu_r = \mu'_r + i\mu''_r$ as functions of the frequency in the range of 8.2–12.4 GHz for the 1 and 10% of prepared nanocomposite dispersed in a polyurethane matrix.

In this nanocomposite, charge polarization happened at the interfaces of CNT–PANI and PANI–(Fe, Co) oxide; this polarization has emerged due to the difference in electrical conductivity of the components and caused negative and positive charges to stack on both sides of the interfaces and produced a nanocapacitor. As it can be seen in Fig. 5a, the amount of stored energy has remained almost constant with increasing frequency in X band; in fact, in the frequency range the electrical dipoles in the structure of the nanocomposite adjusted themselves with the electrical field changes. As Fig. 5b shows, no significant change is observed in the imaginary part of permittivity with increasing frequency. As the theory of materials has been proven, complex permittivity and conductivity are linked by the following relationship [30]:

$$\epsilon = \sigma / 2\pi\epsilon_0 F, \tag{2}$$

where σ and F are conductivity and frequency, respectively, and ϵ_0 is the permittivity of free space. In fact, stable imaginary part of permittivity shows an increase in the electrical conductivity with increase of frequency. Since the amount of applied frequencies of this study was not high; therefore, electric dipoles have the ability to adapt themselves with the applied frequency. Similar to what was expressed for the real part of permittivity, storage mechanism of magnetic field is magnetic dipole polarization in the direction

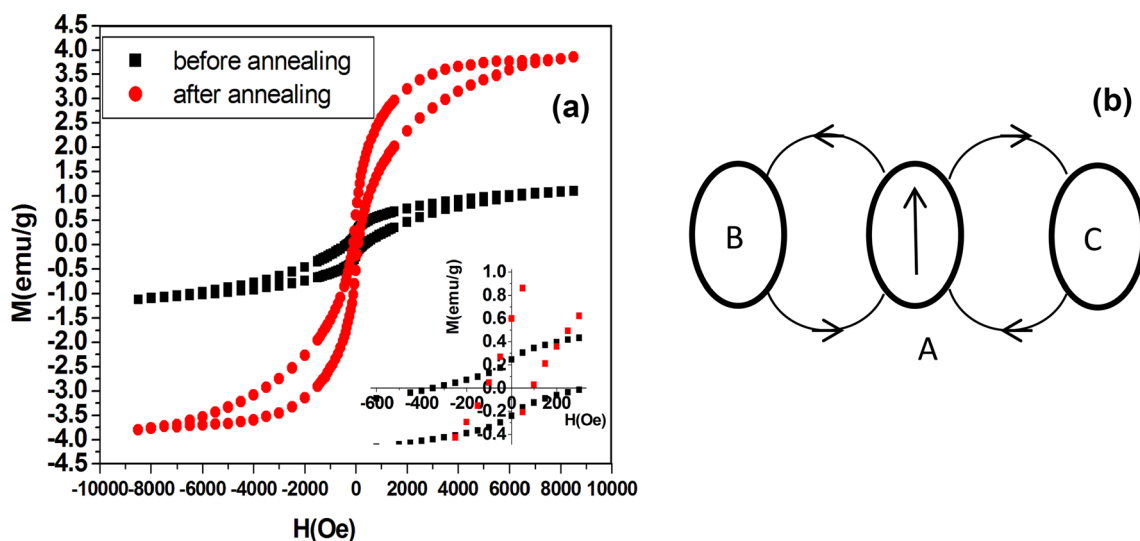


Fig. 4 Magnetic hysteresis loops of synthesized nanocomposite before and after annealing (a) and schematic of particle interactions (b)

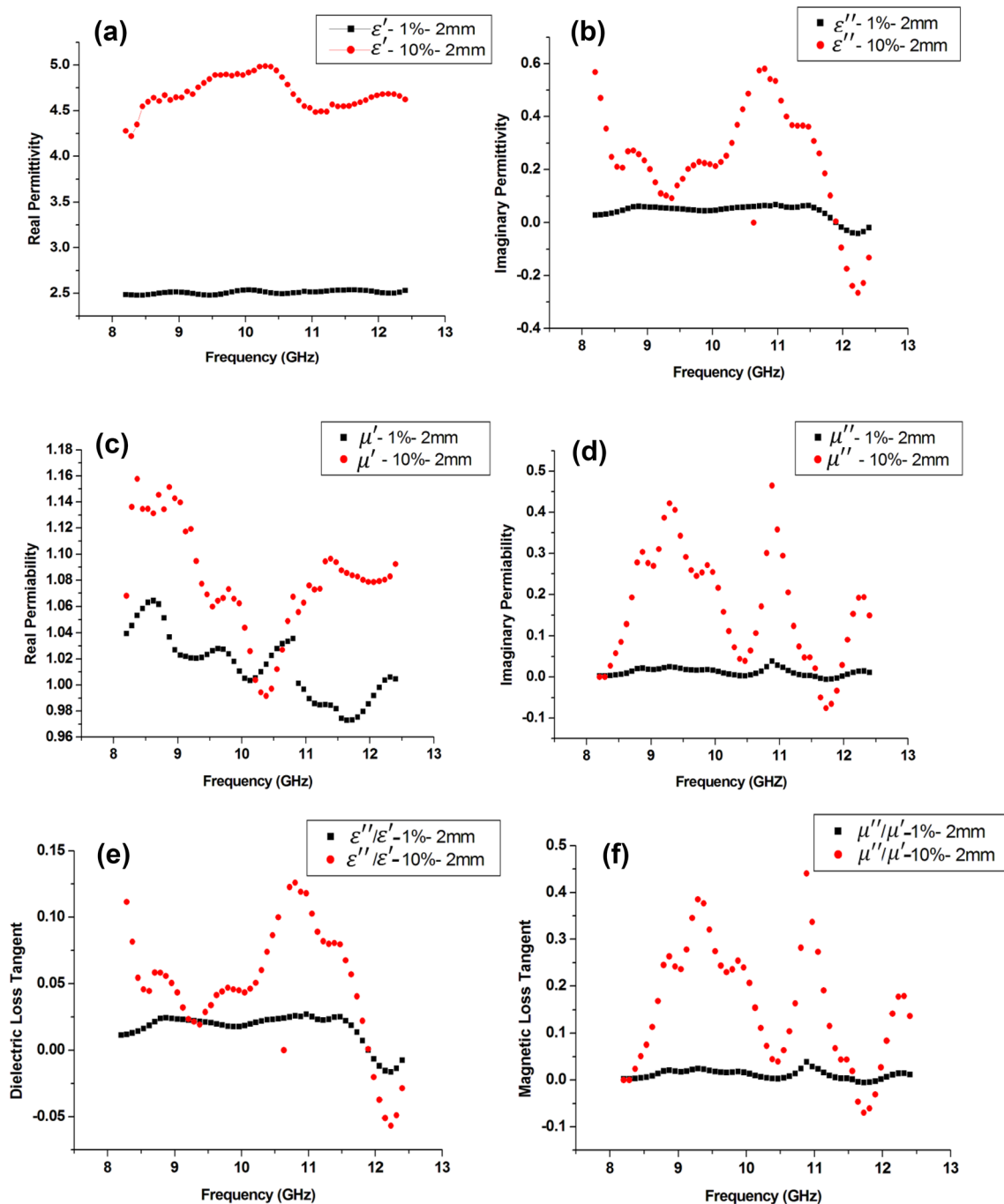


Fig. 5 Variation of electromagnetic characteristics with frequency, **a** ϵ' , **b** ϵ'' , **c** μ' , **d** μ'' , **e** $\tan(\delta_\epsilon)$ and **f** $\tan(\delta_\mu)$

of the applied field. Since magnetic nanoparticles have easy magnetic axes with the least amount of energy; keeping the magnetic dipoles in directions other than easy axes needs energy consumption and leads to the increase of nanoparticles energy levels. This energy will be stored in the structure of nanocomposite in the form of real permeability. From the constant amount of real part of complex permeability in the whole X band range (Fig. 5c), it can be concluded

that the frequency range is not higher than the frequency of the magnetic dipole comfort; so the magnetic dipoles will be able to arrange along with the applied magnetic field; therefore, the mechanism of magnetic dipole polarization contributes in energy storage. The maximum value of the μ'' (Fig. 5d) appears at 9.2 and 10.89 GHz implying occurrence of natural resonance in the present (Fe, Co) oxide microspheres. As it can be seen in the Fig. 5e, f, magnetic



loss tangent is greater than the dielectric loss tangent; this explains the dominance of magnetic loss mechanisms due to the presence of metal oxide nanoparticles and the dielectric loss mechanisms is due to the presence of carbon nanotubes and conductive polyaniline.

Magnetic loss peaks are observed in the Fig. 5f, these peaks show ferromagnetic resonance mechanism. In addition, electrical resistance of iron–cobalt oxide nanoparticles against eddy currents created by magnetic fields is the effective mechanism for wave energy loss. With increasing the percent of nanoparticles in the polyurethane matrix; the number of atoms increases and so the mentioned mechanisms for save and dissipation of energy would act more aggressively and finally more energy will be saved or wasted.

Microwave absorption properties

The reflection loss (RL) of electromagnetic fields radiation under usual incidence of the electromagnetic waves on the surface of a single-layer material on the surface of a conductor has been defined by [31]:

$$R(\text{dB}) = -20 \log \left| \frac{Z_{\text{in}} - 1}{Z_{\text{in}} + 1} \right|, \tag{3}$$

where Z_{in} is the input characteristic impedance at the interface of absorber with air, it is related to dielectric and magnetic parameters of absorbent material by the following equation [31]:

$$Z_{\text{in}} = \sqrt{\frac{\mu_r}{\epsilon_r}} \tan h \left[j \left(\frac{2\pi}{c} \sqrt{\mu_r \epsilon_r} \right) f \cdot d \right], \tag{4}$$

where μ_r and ϵ_r are the complex permeability and permittivity of the composite, respectively; c is the velocity of light in free space, f is the frequency and d is the thickness of the absorber.

In an ideal absorbent material, input impedance is assumed to be 1 ($Z_{\text{in}} = 1$). Figure 6a shows the variation of reflection loss vs. frequency for standard absorber samples with 2 mm thickness. The average of reflection loss along the whole X band and in the absorption samples based on (Fe, Co) oxide–PANI–CNT nanocomposite are around 0.61 and 3.07 dB in samples containing 1 and 10 weight percent of nanocomposite, respectively.

As it can be seen the reflection loss decreases with increase of nanoparticles content. This result can be justified by the truth that enhancement of loading percentage leads to decreasing the possibility of incident microwaves escape; which means high absorption. It can be concluded that, increasing the loading of nanocomposite may lead to the multiple reflections; enlarging the rate of absorption and the increasing RL peaks from 9.33 to 11.97 GHz. Reflection be affected of polarization of the incident waves. It has been proved that the parallel waves and perpendicular waves have different polarization and this leads to different reflection coefficients [32].

Two main mechanisms involved in the increasing of protective effect: the mechanism of reflection due wave impedance step and the mechanism of absorption in which electromagnetic wave energy is converted to other energy such as thermal energy [33].

The potency of an absorber to absorption depends on many parameters such as: (1) the least amount of reflection

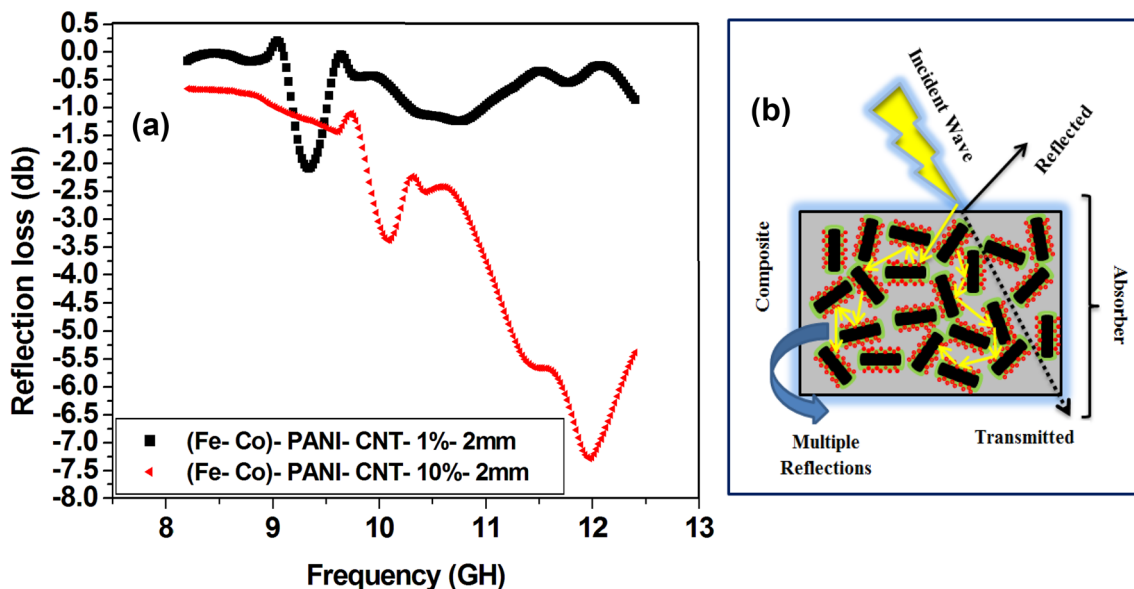


Fig. 6 Variation of reflection loss vs. frequency for single layer absorber samples with a. 2 mm thickness, concentration of 1 and 10% (a), schematic presentation of the absorption mechanism (b)

from the surface of the adsorbent and (2) the greatest amount of wave sliding inside adsorbent influences in the effective absorption of an adsorbent.

To minimize the reflection of the incident wave to the absorber surface; we should try to get the impedance of free space close to impedance of the adsorbent. By increasing the impedance matching; the amount of absorption increases and thus the effectiveness of dielectric loss and magnetic loss will be greater and in this research magnetic loss and dielectric loss have been together. There are two mechanisms for enhanced wave absorption: (1) electrical polarization of interface and (2) multiple scattering by available defects in the structure of matter [31]. Hence, the composite composed of two dielectric materials (CNT–PANI) and magnetic material (Fe, Co) oxide can be used as a high operation and light weight microwave absorber wherein the mechanism of electrical polarization of interface has a positive effect on increasing its absorption ability. C–C bound in carbon nanotubes actually acts as a short circuit, therefore causes the high protective and low reflection effect against the incident waves [34].

From these results, it can be understood that the sketch of multicomponent absorber by various fillers with varied electromagnetic absorption mechanisms is very helpful to raise the reflection loss of the absorber built. Furthermore optimization of the thickness and the loading percentage of dispersed nanoparticles in matrix may lead to enhance reflection losses.

Conclusions

In this research novel magnetic-dielectric nanocomposite [(Fe, Co) oxide–Pani–CNT] with lightweight, thin-layer properties has been successfully synthesized via a simple, low cost and effective chemical process. We have also successfully developed a core–shell and sub-cluster structures. The structural and compound characterization was done by FTIR, XRD, SEM and TEM. The magnetic and optical properties were also investigated by VSM and UV–Vis, respectively. Finally, we investigated the electromagnetic and microwave absorption properties of the composite in the X band region. From the results it can be inferred that the nice complementarity among magnetic and dielectric loss modifies compliance of the impedance status, which more helps in the absorption and debilitation of the waves. Dielectric loss can be resulted from the polarization in the nanocomposite components and their interface, and ferromagnetic resonance losses and attenuation of microwave within the walls of magnetic domains causes magnetic loss. The samples of absorption with 1 and 10% loading and 2 mm thick showed maximum RL of -2.14 dB at 9.33 GHz and -7.32 dB at 11.97 GHz, respectively.

Open Access This article is distributed under the terms of the Creative Commons Attribution 4.0 International License (<http://creativecommons.org/licenses/by/4.0/>), which permits unrestricted use, distribution, and reproduction in any medium, provided you give appropriate credit to the original author(s) and the source, provide a link to the Creative Commons license, and indicate if changes were made.

References

- Kimura, S., Kato, T., Hyodo, T., Shimizu, Y., Egashira, M.: Electromagnetic wave absorption properties of carbonyl iron-ferrite/PMMA composites fabricated by hybridization method. *J. Magn. Mater.* **312**(1), 181–186 (2007)
- Wu, K.H., Huang, W.C., Wang, G.P., Wu, T.R.: Effect of pH on the magnetic and dielectric properties of SiO₂/NiZn ferrite nanocomposites. *Mater. Res. Bull.* **40**(10), 1822–1831 (2005)
- Dosoudil, R., Ušáková, M., Franek, J., Sláma, J., Olah, V.: RF electromagnetic wave absorbing properties of ferrite polymer composite materials. *J. Magn. Mater.* **304**(2), e755–e757 (2006)
- Abbas, S.M., Dixit, A.K., Chatterjee, R., Goel, T.C.: Complex permittivity, complex permeability and microwave absorption properties of ferrite–polymer composites. *J. Magn. Mater.* **309**(1), 20–24 (2007)
- Li, S., et al.: Aqueous zinc–polyaniline secondary battery. *Synth. Met.* **158**(6), 242–245 (2008)
- Kilmartin, P.A., Martinez, A., Bartlett, P.N.: Polyaniline-based microelectrodes for sensing ascorbic acid in beverages. *Curr. Appl. Phys.* **8**(3), 320–323 (2008)
- Ogurtsov, N.A., et al.: Corrosion inhibition of aluminum alloy in chloride mediums by undoped and doped forms of polyaniline. *Synth. Met.* **143**(1), 43–47 (2004)
- Håkansson, E., Amiet, A., Kaynak, A.: Dielectric characterization of conducting textiles using free space transmission measurements: accuracy and methods for improvement. *Synth. Met.* **157**(24), 1054–1063 (2007)
- Stafström, S., et al.: Polaron lattice in highly conducting polyaniline: theoretical and optical studies. *Phys. Rev. Lett.* **59**(13), 1464 (1987)
- Zuo, F., et al.: AC conductivity of emeraldine polymer. *Phys. Rev.* **B39**(6), 3570 (1989)
- Hsieh, T.-H., Ho, K.-S., Huang, C.-H., Wang, Y.-Z., Chen, Z.-L.: Electromagnetic properties of polyaniline/maghemite nanocomposites: I. The effect of re-doping time on the electromagnetic properties. *Synth. Met.* **156**(21), 1355–1361 (2006)
- Ameen, S., Ali, V., Zulfuqar, M., Mazharul Haq, M., Husain, M.: Preparation and measurements of electrical and spectroscopic properties of sodium thiosulphate doped polyaniline. *Curr. Appl. Phys.* **9**(2), 478–483 (2009)
- Phang, S.-W., Hino, T., Abdullah, M.H., Kuramoto, N.: Applications of polyaniline doubly doped with *p*-toluene sulphonic acid and dichloroacetic acid as microwave absorbing and shielding materials. *Mater. Chem. Phys.* **104**(2), 327–335 (2007)
- Wang, Z., Bi, H., Liu, J., Sun, T., Wu, X.: Magnetic and microwave absorbing properties of polyaniline/ γ -Fe₂O₃ nanocomposite. *J. Magn. Mater.* **320**(16), 2132–2139 (2008)
- Wang, C., Lv, R., Kang, F., Gu, J., Xuchun, G., Wu, D.: Synthesis and application of iron-filled carbon nanotubes coated with FeCo alloy nanoparticles. *J. Magn. Mater.* **321**(13), 1924–1927 (2009)
- Fan, Z., Luo, G., Zhang, Z., Zhou, L., Wei, F.: Electromagnetic and microwave absorbing properties of multi-walled carbon nanotubes/polymer composites. *Mater. Sci. Eng. B* **132**(1), 85–89 (2006)



17. Bauhofer, W., Kovacs, J.Z.: A review and analysis of electrical percolation in carbon nanotube polymer composites. *Compos. Sci. Technol.* **69**(10), 1486–1498 (2009)
18. Zhou, Y., He, B., Zhou, W., Huang, J., Li, X., Wu, B., Li, H.: Electrochemical capacitance of well-coated single-walled carbon nanotube with polyaniline composites. *Electrochim. Acta* **49**(2), 257–262 (2004)
19. O’Connell, M.J., Boul, P., Ericson, L.M., Huffman, C., Wang, Y., Haroz, E., Kuper, C., Tour, J., Ausman, K.D., Smalley, R.E.: Reversible water-solubilization of single-walled carbon nanotubes by polymer wrapping. *Chem. Phys. Lett.* **342**(3), 265–271 (2001)
20. Guo, L., Peng, Z.: One pot synthesis of carbon nanotube-polyaniline-gold nanoparticle and carbon nanotube-gold nanoparticle composites by using aromatic amine chemistry. *Langmuir* **24**(16), 8971–8975 (2008)
21. Lee, H.-Y., Vogel, W., Chu, P.P.-J.: Nanostructure and surface composition of Pt and Ru binary catalysts on polyaniline-functionalized carbon nanotubes. *Langmuir* **27**(23), 14654–14661 (2011)
22. Dhand, C., Arya, S.K., Singh, S.P., Singh, B.P., Datta, M., Malhotra, B.D.: Preparation of polyaniline/multiwalled carbon nanotube composite by novel electrophoretic route. *Carbon* **46**(13), 1727–1735 (2008)
23. Quillard, S., Louam, G., Buisson, J.P., Boyer, M., Lapkowski, M., Pron, A., Lefrant, S.: Vibrational spectroscopic studies of the isotope effects in polyaniline. *Synth. Met.* **84**(1), 805–806 (1997)
24. Maensiri, S., Masingboon, C., Boonchom, B., Seraphin, S.: A simple route to synthesize nickel ferrite (NiFe₂O₄) nanoparticles using egg white. *Scr. Mater.* **56**(9), 797–800 (2007)
25. Jeevananda, T., Kim, N.H., Heo, S.-B., Lee, J.H.: Synthesis and characterization of polyaniline-multiwalled carbon nanotube nanocomposites in the presence of sodium dodecyl sulfate. *Polym. Adv. Technol.* **19**(12), 1754–1762 (2008)
26. Shaikh, P.A., Kambale, R.C., Rao, A.V., Kolekar, Y.D.: Structural, magnetic and electrical properties of Co–Ni–Mn ferrites synthesized by co-precipitation method. *J. Alloys Comp.* **492**(1), 590–596 (2010)
27. Cullity, B.D., Graham, C.D.: Introduction to magnetic materials. Wiley, New York (2011)
28. Chen, D.-X., Pascu, O., Roig, A., Sanchez, A.: Size analysis and magnetic structure of nickel nanoparticles. *J. Magn. Magn. Mater.* **322**(24), 3834–3840 (2010)
29. Ramo, S., Whinnery, J.R., Van Duzer, T.: Fields and waves in communication electronics. Wiley, New York (2008)
30. Ghasemi, A., Hossienpour, A., Morisako, A., Saatchi, A., Salehi, M.: Electromagnetic properties and microwave absorbing characteristics of doped barium hexaferrite. *J. Magn. Magn. Mater.* **302**(2), 429–435 (2006)
31. Sun, S., He, Q., Xiao, S., Xu, Q., Li, X., Zhou, L.: Gradient-index meta surfaces as a bridge linking propagating waves and surface waves. *Nat. Mater.* **11**(5), 426–431 (2012)
32. Micheli, D., Pastore, R., Apollo, C., Marchetti, M., Gradoni, G., Primiani, V.M., Moglie, F.: Broadband electromagnetic absorbers using carbon nanostructure-based composites. *IEEE Trans. Microw. Theory Tech.* **59**(10), 2633–2646 (2011)
33. Micheli, D., Vricella, A., Pastore, R., Delfini, A., Giusti, A., Albano, M., Marchetti, M., Moglie, F., Mariani Primiani, V.: Ballistic and electromagnetic shielding behaviour of multifunctional Kevlar fiber reinforced epoxy composites modified by carbon nanotubes. *Carbon* **104**, 141–156 (2016)
34. Micheli, D., Apollo, C., Pastore, R., Barbera, D., Morles, R.B., Marchetti, M., Gradoni, G., Primiani, V.M., Moglie, F.: Optimization of multilayer shields made of composite nanostructured materials. *IEEE Trans. Electromagn. Compat.* **54**(1), 60–69 (2012)

Publisher’s Note Springer Nature remains neutral with regard to jurisdictional claims in published maps and institutional affiliations.

